

Gold-reinforced silver nanoprisms on optical fiber tapers—A new base for high precision sensing

T. Wieduwilt, M. Zeisberger, M. Thiele, B. Doherty, M. Chemnitz, A. Csaki, W. Fritzsche, and M. A. Schmidt

Citation: *APL Photonics* **1**, 066102 (2016); doi: 10.1063/1.4953671

View online: <http://dx.doi.org/10.1063/1.4953671>

View Table of Contents: <http://scitation.aip.org/content/aip/journal/app/1/6?ver=pdfcov>

Published by the [AIP Publishing](#)

Articles you may be interested in

[Quantum sized Ag nanocluster assisted fluorescence enhancement in Tm³⁺-Yb³⁺ doped optical fiber beyond plasmonics](#)

Appl. Phys. Lett. **107**, 233107 (2015); 10.1063/1.4937387

[Plasmon enhanced broadband optical absorption in ultrathin silicon nanobowl array for photoactive devices applications](#)

Appl. Phys. Lett. **107**, 013107 (2015); 10.1063/1.4926627

[Multi-component nanocomposite for all-optical switching applications](#)

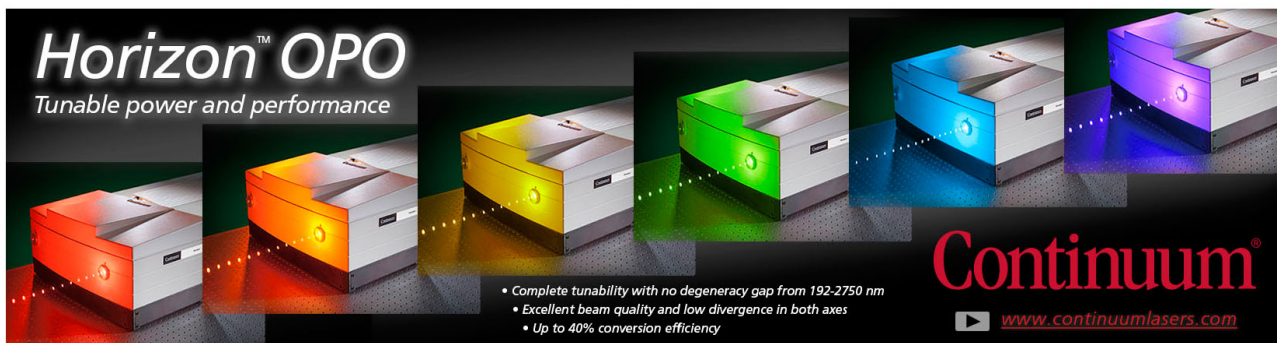
Appl. Phys. Lett. **99**, 141113 (2011); 10.1063/1.3646376

[Internal specular reflection from nanoparticle layers on the end face of optical fibers](#)

J. Appl. Phys. **109**, 103114 (2011); 10.1063/1.3583582

[Optical fiber affinity biosensor based on localized surface plasmon resonance](#)

Appl. Phys. Lett. **85**, 4231 (2004); 10.1063/1.1812583



Horizon™ OPO
Tunable power and performance

• Complete tunability with no degeneracy gap from 192-2750 nm
• Excellent beam quality and low divergence in both axes
• Up to 40% conversion efficiency

Continuum®
www.continuumlasers.com

The advertisement features a row of five Continuum Horizon OPO laser units, each emitting a different color of light: red, orange, yellow, green, and blue. The units are shown from a three-quarter perspective, highlighting their compact, boxy design. The background is dark, making the glowing lasers stand out.

Gold-reinforced silver nanoprisms on optical fiber tapers—A new base for high precision sensing

T. Wieduwilt,^{1,a} M. Zeisberger,¹ M. Thiele,¹ B. Doherty,^{1,2} M. Chemnitz,^{1,2}
 A. Csaki,¹ W. Fritzsche,^{1,2} and M. A. Schmidt^{1,2,3}

¹Leibniz Institute of Photonic Technology e.V., Albert-Einstein-Str.9, 07745 Jena, Germany

²Abbe Center of Photonics, Friedrich-Schiller-University, Max-Wien-Platz 1,
 07743 Jena, Germany

³Otto Schott Institute of Material Research, Friedrich-Schiller-University, Fraunhoferstr.6,
 07743 Jena, Germany

(Received 26 April 2016; accepted 30 May 2016; published online 13 July 2016)

Due to their unique optical properties, metallic nanoparticles offer a great potential for important applications such as disease diagnostics, demanding highly integrated device solutions with large refractive index sensitivity. Here we introduce a new type of monolithic localized surface plasmon resonance (LSPR) waveguide sensor based on the combination of an adiabatic optical fiber taper and a high-density ensemble of immobilized gold-reinforced silver nanoprisms, showing sensitivities up to 900 nm/RIU. This result represents the highest value reported so far for a fiber optic sensor using the LSPR effect and exceeds the corresponding value of the bulk solution by a factor of two. The plasmonic resonance is efficiently excited via the evanescent field of the propagating taper mode, leading to pronounced transmission dips (−20 dB). The particle density is so high (approx. 210 particle/ μm^2) that neighboring particles are able to interact, boosting the sensitivity, as confirmed by qualitative infinite element simulations. We additionally introduce a qualitative model explaining the interaction of plasmon resonance and taper mode on the basis of light extinction, allowing extracting key parameters of the plasmonic taper (e.g., modal attenuation). Due to the monolithic design and the extremely high sensitivity we expect our finding to be relevant in fields such as biomedicine, disease diagnostics, and molecular sensing. © 2016 Author(s). All article content, except where otherwise noted, is licensed under a Creative Commons Attribution (CC BY) license (<http://creativecommons.org/licenses/by/4.0/>). [<http://dx.doi.org/10.1063/1.4953671>]

I. INTRODUCTION

Metallic nanoparticles (meNPs) can show a very distinct optical response in the visible and near infrared part of the spectrum in case their diameters fall into the nanoscale domain. Here, an incident electromagnetic wave can excite the electrons inside the metal, which leads to a plasma-type oscillation of the electron ensemble, i.e., to the so-called localized surface plasmon resonance (LSPR). Particular for deep subwavelength meNP diameters, the optical response resembles that of a point dipole with a precisely defined phase retardation and orientation of the dipole axis. In comparison to their propagating counterparts in planar and cylindrical geometries,^{1–3} LSPR shows extreme strong field confinements, i.e., their penetration depth into the surrounding dielectric is of the order of tens of nanometers only,⁴ which makes them attractive for detecting nanoscale environmental changes which, for instance, are imposed by chemical reactions.

Colloidal meNPs have shown to be extremely useful particularly from the application perspective, since they are fabricated on large scales using chemical synthesis, i.e., a bottom-up approach, giving rise to large sample yields in contrast to, e.g., lithographic fabrication methods. Together

^aAuthor to whom correspondence should be addressed. Electronic mail: torsten.wieduwilt@ipht-jena.de



with the above-mentioned strong field confinement, this particular feature has made them attractive for applications such as biomedicine^{5,6} or nanoscale sensing.⁷ One important application example of colloidal NPs is the detection of molecular events via an imposed change of the LSPR: The strong field confinement allows detecting small refractive index (RI) changes of the surrounding analyte in a nanoscale environment around the NP via measuring the spectral shift of LSPR. The key parameter characterizing this phenomenon is the sensitivity S , which is defined by the ratio between the spectral shift of the LSPR $\Delta\lambda_R$ and the change of the refractive index in the vicinity of the meNP Δn ($S = \Delta\lambda/\Delta n$).⁸ As a result functionalization of plasmonic NPs with receptor (capture) molecules (e.g., proteins, antigens, and ssDNA) allows the identification of selective molecular bindings effect (e.g., antigen-antibody or DNA-DNA binding), which represents a key for, e.g., disease diagnosis.⁹⁻¹¹ Another important application field of colloidal meNPs is cancer therapy, where first results indicate that laser-induced heating of NPs via strong energy dissipation can help to locally destroy pathogenic tissue.¹²⁻¹⁴

Many of the currently employed plasmonic colloidal systems rely on noble metals such as gold or silver due to low intrinsic ohmic damping, which ultimately yields in strong LSPRs in the visible and near infrared.⁴ Up to date, the most widely used colloidal NPs are gold nanospheres due to long-term stability and straightforward synthesis pathway. However, these nanospheres reveal comparably low RI sensitivity (of the order of 80 nm/RIU),⁸ making them unattractive in case very small amounts of species are to be detected. This problem can be addressed by using NPs with large aspect ratios, which can show up to one order of magnitude larger sensitivity values and can be used for molecular sensing via local molecular binding.¹⁵ With respect to application in biosensing and medicine, meNPs with “pointish”-type shapes such as cubes or stars¹⁶ have recently attracted a lot of attention, since they give rise to extraordinary high sensitivities in case the analyte to be detected locally binds at the sharp edges of the NP.

For practical reasons colloidal nanoparticles are typically immobilized on solid surfaces and are investigated using, e.g., dark field microscopy,^{17,18} whereas the incident light excites the LSPR and the scattered light is collected via high numerical aperture objectives. This approach has found wide-spread use but lacks monolithic and straightforward device integration and the possibility of investigating large ensembles of meNPs.

One promising scheme to address this issue is to integrate colloidal meNPs into photonic waveguiding system, which for instance can be realized by placing the NPs into the evanescent fields of an optical mode. Here, the LSPRs are excited via the tails of the propagating modes and the spectral properties of the plasmonic resonance can be measured via examining the waveguide transmission. This hybrid scheme has been successfully implemented within the scope of planar photonics, as for instance it was shown that LSPRs can be coupled to the modes of slab waveguides; in this case the meNPs were deposited on top of the waveguide, leading to a substantial transmission modification.^{19,20}

However, planar waveguides reveal intrinsic problematic features such as high optical loss due to, e.g., surface roughness or surface state absorption, the prerequisite of complex fabrication technology and incompatibility to fiber optical technology. One attractive solution to the mentioned problems is to combine meNP and optical fibers on the basis of fiber-optical tapers: These highly integrated photonic elements consist of down-tapered optical fibers to diameters so small that the evanescent field of the optical mode penetrates the surrounding material, i.e., the analyte. Tapers have been successfully employed for exciting both propagating surface plasmon-polaritons²¹⁻²⁵ and localized plasmonic modes, whereas in the latter case only NPs with comparably low sensitivity have been employed (e.g., gold nanospheres (diameter 24 nm) sensitivity of ~ 51 nm/RIU)²⁶ mostly using single mode fibers. Besides the mentioned tapers, the evanescent field can be also accessed using techniques such as mechanical stripping of the cladding, which was used for plastic-clad multimode fibers²⁷⁻³¹ and chemical removal of the cladding via etching used for silica clad multimode³² and single mode fibers, respectively.³³ Other types of fiber-optic sensors not using plasmonic excitations rely on effects such as long-period gratings (1500 nm/RIU),³⁴ coupling to modes beyond modal cut-off (301 000 nm/RIU),³⁵ directional mode coupling (3200 nm/RIU),³⁶ multimodal interference (667 nm/RIU),³⁷ focused ion-beam

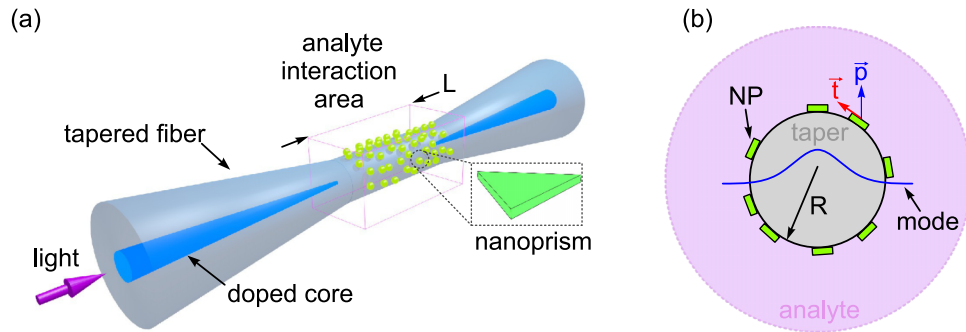


FIG. 1. (a) Schematic of the plasmonic fiber optical taper coated with highly sensitive silver-gold nanoprisms in the region of the taper waist. The magenta box indicates the domain the analyte is applied. (b) Cross section of the plasmonic taper in the domain the nanoprisms are deposited. The small green structures indicate the nanoprisms on the surface of the taper and the purple curve represents the propagating of fundamental optical taper mode. The two vectors indicate the local orientations of the polarization vector of the guided mode \vec{p} and the vector parallel to the film surface of the NP \vec{t} .

machined Fabry-Perot cavities (1130 nm/RIU, 1150 nm/RIU),^{38,39} and laser-written Bragg gratings (10 nm/RIU).⁴⁰

Here we show that silver nanoprisms immobilized on an adiabatic optical fiber taper Fig. 1(a) result in a novel hybrid plasmonic-photonic system with extraordinary high sensitivity values of about 900 nm/RIU, which exceeds that of the corresponding bulk solution by a factor of two. This key feature of our system results from the fact that the taper allows precise engineering of the interaction between LSPR and taper mode. In fact the fraction of evanescent field outside the taper has been adjusted such that meNP densities sufficiently high for interaction of the LSPRs of neighboring meNPs can be established on the taper surface, which results in substantially higher sensitivities than compared to the case of meNPs dispersed in solution.

Moreover, strong transmission dips with extinction ratios of up to 20 dB are observed, making the taper approach particular attractive for index sensing. Since the LSPRs are detected via analyzing the change of the transmission through the taper, our system represents a highly integrated and straightforward-to-use approach, which has the potential to give rise to a full monolithic sensor being compatible with fiber circuitry. The taper and the meNP immobilization are straightforward to conduct and due to mm-long interaction length our sensor is of macroscopic scale, making it attractive from the handling perspective.

In addition to all relevant experimental details, we present a fitting model which allows explaining the interaction of LSPR and taper mode on the basis of light extinction and extracting key characteristics of the plasmonic taper such as the modal attenuation. We also present simulations from a qualitative scattering model, showing that interparticle interaction leads to a substantial increase in RI sensitivity in the case of high particle densities.

II. THEORETICAL BACKGROUND

The working principle of the meNP-enhanced fiber taper presented here relies on the interaction of the LSPR with the propagating mode inside the taper. Within the taper waist, the evanescent field of the guided wave penetrates the analyte and excites the LSPRs of the meNPs on the surface of the taper. The corresponding fraction of electromagnetic energy is in fact removed from that of the optical mode (via scattering and absorption of the nanoparticle) and as a result strong transmission dips are observed. A key feature of the taper concept is that the fraction of field in the analyte, i.e., the fraction exciting the LSPR, can be precisely adjusted via the taper diameter, ultimately allowing for investigating meNP ensembles with extremely high coverage. For the structure discussed here the fraction of evanescent field in the analyte is only 0.1% in case water is surrounding the taper (at 700 nm), allowing to examine meNP ensemble with a density so high that neighboring meNPs interact.

The attenuation coefficient of the mode propagating inside the taper γ (i.e., LSPR-induced extinction coefficient) can be described by a line integral along the circumference of the taper, leading to

$$\gamma = \oint_{r=R} \frac{N\sigma(\phi, \Delta\lambda)}{A_{\text{eff}}(r, \phi, \Delta\lambda)} dl, \quad (1)$$

with the density of the nanoprisms N (number of meNPs per unit area), the relative wavelength $\Delta\lambda = \lambda - \lambda_R$ (λ : vacuum wavelength, λ_R : LSPR resonance wavelength), the azimuthal angle dependent extinction cross section $\sigma(\phi)$, and the taper radius R . In case of an anisotropic meNP (which holds for the nanoprisms considered here), the excitation of the LSPR depends on the relative orientation of meNP (defined here as the unity vector parallel to the meNP surface \vec{t}) and unity polarization vector of the guided mode \vec{p} at the location of the meNP (Fig. 1(b)). Since the extinction cross section is generally defined with respect to intensity,⁴¹ we define $\sigma(\phi) = \sigma_0(\vec{t} \cdot \vec{p})^2$ including the bulk extinction cross section σ_0 , which can either be determined from simulating the scattering properties of a single meNP or from measuring the particle extinction. Here we determined σ_0 from bulk solution (subsequently denoted as σ_s), which is to some extent a different situation compared to plasmonic taper case. In solution the particles are randomly orientated along all three spatial directions, whereas in the taper case the particles lie on the taper surface, i.e., are preferentially oriented normal to the taper axis. This orientation imposes a reduced dimensionality in the taper situation ($3 \rightarrow 2$) leading to a larger cross section (i.e., more particles contribute to the overall extinction), which can be accounted for by the following substitution: $\sigma_t = \sigma_s \cdot 3/2$. This ansatz assumes that the maximum LSPR excitation is achieved for parallel orientation of \vec{p} and \vec{t} , whereas there is negligible contribution of the LSPR excitation in the perpendicular direction. This leads to $\sigma_t(\phi) = \sigma_t \cos^2 \phi$ (ϕ : angle between \vec{t} and \vec{p}) and is in correspondence with the qualitative planar waveguide simulations shown later, which shows that the strongest LSPR excitation is achieved for TE-polarization, i.e., $\phi = 0$. The parameter $A_{\text{eff}}(r, \phi, \Delta\lambda)$ refers to the area of the mode on the surface of the taper^{42,43} and is associated with the Poynting vector distribution of the mode under investigation S_z ,

$$A_{\text{eff}}(R, \Delta\lambda) = \frac{\int_{A=\infty} S_z(r, \phi, \Delta\lambda) dA}{S_z(r = R, \phi, \Delta\lambda)}. \quad (2)$$

The effective mode area depends on the azimuthal coordinate, suggesting that γ depends on the azimuthal position of meNP on the taper surface. In the situation investigated here, however, the taper diameters are comparably large, and hence the guided HE_{11} mode has a Gaussian type mode distribution with only a small azimuthal dependence, allowing to define an average and constant effective area $\bar{A}_{\text{eff}} = 2 \int S_z dA / (S_z(r = R, \phi = 0^\circ, \Delta\lambda) + S_z(r = R, \phi = 90^\circ, \Delta\lambda))$. Due to the high symmetry of the cylindrical geometry, \bar{A}_{eff} has a full analytic form since S_z can be expressed by a single analytic function.^{44,45} As a result of independence of A_{eff} on azimuthal angle and the simple mathematical form of $\sigma_t(\phi)$, the line integral Eq. (1) can be equated analytically, leading to

$$\gamma(\Delta\lambda) = \frac{N\sigma_t(\Delta\lambda)}{\bar{A}_{\text{eff}}(\Delta\lambda)} \pi R. \quad (3)$$

This allows expressing the transmitted power P_T through the plasmonic taper of the length L via the following equation:

$$P_T(\Delta\lambda) = P_0 \exp\left(-\frac{N\sigma_t(\Delta\lambda)}{\bar{A}_{\text{eff}}(\Delta\lambda)} \pi RL\right), \quad (4)$$

with the input power P_0 .

It is interesting to note that Eq. (4) clearly shows that the modal attenuation is in fact determined by the ratio of the two areas involved, i.e., σ_t/A_{eff} , which emphasizes that tuning the optical mode properties allows the engineering of the transmission properties (inset of Fig. 2).

This tunability feature appears even more pronounced when investigating the ratio R/A_{eff} (Fig. 2) including all geometric parameters determined by the taper and showing that argument

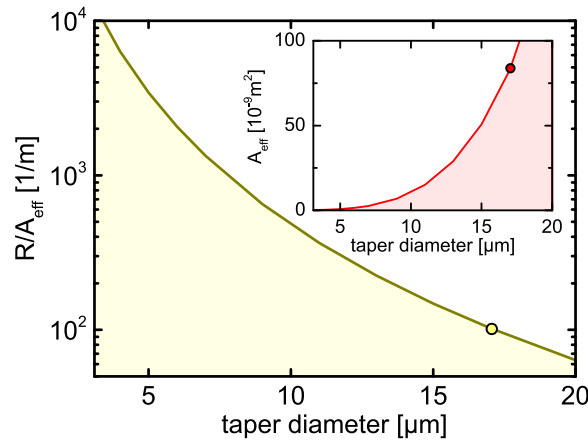


FIG. 2. Dependence of R/A_{eff} ratio on taper diameter at a fixed wavelength of 740 nm (taper material: silica, surrounding analyte: water). The inset shows the effective mode cross section as a function of taper diameter. The points in both plots indicate the configuration used in the experiment (taper diameter 17 μm).

of the exponential function of P_T (Eq. (4)) can be tuned over two orders of magnitude only by changing the taper diameter, which in fact allows studying a broad range of NP densities.

III. FABRICATION AND MEASUREMENT METHOD

For the investigation presented here, we used gold-reinforced silver nanoprisms with approximate dimensions of 40 ± 20 nm and a thickness of 9 ± 2 nm, being chemically fabricated using a combination of seed particle synthesis and subsequent nanoprism growth (inset of Fig. 3(a), see supplementary material, Sec. I⁵¹). To avoid catalytic oxidation (etching) of the silver in particular at the edges of the nanoprisms,^{46,47} we overgrow the nanoprism edges with a thin gold layer, which is a well-known approach to stabilize silver NPs,^{48,49} for instance, by using them in physiological conditions⁵⁰ (see supplementary material,⁵¹ Sec. I, preparation of mNPs). This step is essential for the temporal stability of our hybrid system, as otherwise the oxidation would impose a morphology

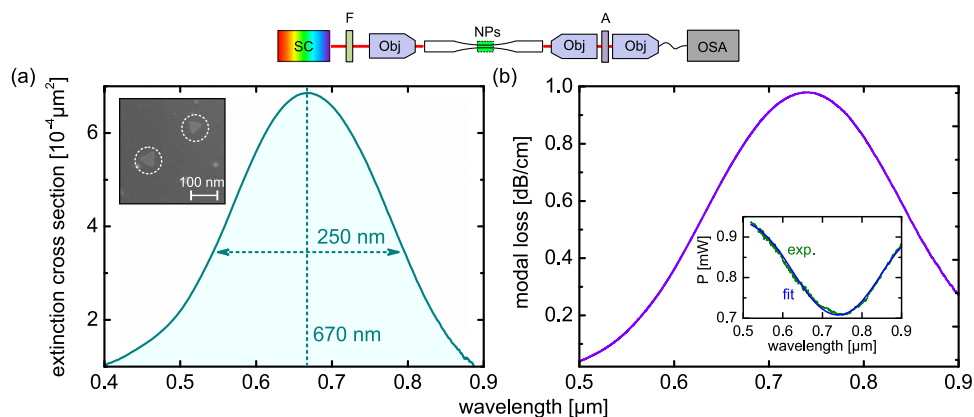


FIG. 3. (a) Spectral distribution of the extinction cross section of the localized plasmonic resonance of the nanoprisms, measured in aqueous solution. The inset exemplarily shows a scanning electron micrograph (SEM) of two silver nanoprisms (highlighted by the dashed circles) deposited onto a planar glass surface. The vertical (horizontal) dashed line represents the center resonance wavelength (FWHM peak width). (b) Spectral distribution of the modal attenuation calculated using the plasmonic taper transmission function defined in Eq. (3). The inset shows the experimentally obtained data (green) and the fit (blue) in case water is used as analyte. The sketch above both plots shows the experimental transmission setup used to determine the transmission properties of the plasmonic tapers (SC: supercontinuum source, F: water filter, Obj: objective, Nikon CF Plan 50 \times /0.55WD 8.7).

change of the nanoprisms (from triangular to disk shape) resulting in a substantially reduced RI sensitivity. We observe that the nanoprisms have triangular as well as hexagonal shapes.

The fiber tapers have been fabricated from silica-based step-index fibers (Nufern HP780, cut-off wavelength 730 nm) and were tapered down over length of ~ 84 mm (using a Vytran GPX 3200, total fiber length: 25 cm). The waist had a length of ~ 14 mm (constant diameter section) and a radius of $R = 8.5 \mu\text{m}$. The two transition zones had lengths of 35 mm to provide adiabaticity, i.e., avoid higher-order mode excitation, giving rise to a clean fundamental mode in the waist section. Within that section, the influence of the doped core on the propagating modes is so small that it can be neglected. The mode inside the waist can thus be represented by the fundamental (HE_{11}) mode of cylindrical silica strand in either air or the analyte. The nanoprisms were attached to the taper using an aminosilane linker (see supplementary material,⁵¹ Sec. III, preparation of fiber probes).

The nanoprisms were deposited over the entire length of the waist ($L = 14$ mm), whereas the density of the nanoprisms N was coarsely controlled via changing the immobilization time. Due to the comparably broad size distribution of the nanoprisms, it turned out to be difficult to quantify the exact value of N for one fixed deposition time. For instance, in the case of 17 min immobilization time (in the following referred as “long” immobilization time), the particle density was in the order of $(210 \pm 30) \text{ NPs}/\mu\text{m}^2$, whereas a 90 s deposition (“short” immobilization time) yields $N \approx (50 \pm 30) \text{ NPs}/\mu\text{m}^2$.

To determine the transmission of the plasmonic fiber taper we used the following experimental setup (top image of Fig. 3(a)): Light from a supercontinuum source SC (SuperK Compact, bandwidth 400 nm–1.8 μm) was coupled into the fiber using a microscope objective (Nikon CF Plan, 50 \times), and the spectral distribution of the transmitted light was measured by an OSA (Ando, AQ6315A, resolution 2 nm). To prevent sample heating and thus an undesired change of the analyte RI, a 1-cm cuvette filled with water acting as IR blocking filter was inserted just after the output of the light source to avoid absorption via infrared light. The spectra were normalized to corresponding spectra of tapers without meNPs in air, whereas control measurements show no difference in transmission between uncoated tapers in air and water.

The RI sensitivity was determined by measuring the LSPR resonance wavelength (transmission dips) in case the meNP-enhanced taper is immersed in different RI environments. Here we used as analyte a series of D-glucose-water solutions with RI in the range between 1.34 and 1.38 (see supplementary material,⁵¹ Sec. II, optical characterization). The wavelength of the LSPR (transmission dips, for instance Fig. 4) was taken from the transmission curves and plotted as a function of analyte index (at λ_R), allowing the determination of the corresponding slope, i.e., sensitivity (see, for instance, Fig. 5). The sensitivity of the nanoprisms in bulk solution was measured in an analogous

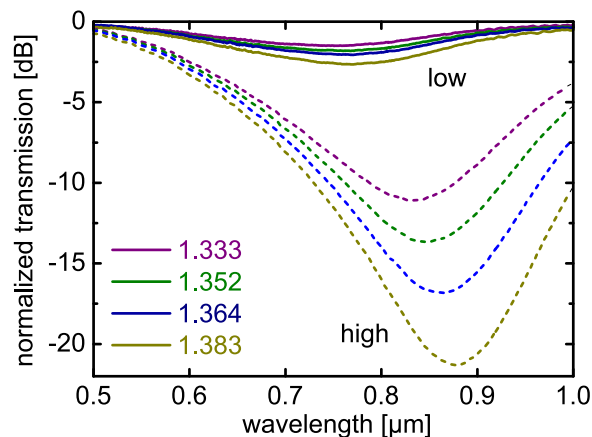


FIG. 4. Wavelength dependence of the measured normalized transmission through the plasmonic taper coated with the nanoprisms. The transmission of tapers with either high (indicated by the dashed lines) or low (indicated by the solid lines) nanoparticle densities has been investigated for four different values of analyte refractive index (numbers refer to the bulk refractive index of the respective analyte at 589 nm). Purple: 1.333, green: 1.352, blue: 1.364, dark yellow: 1.383).

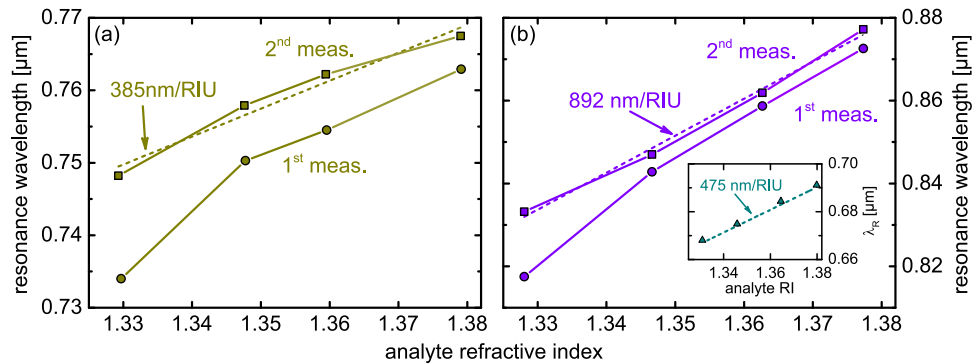


FIG. 5. Resonance wavelength (spectral position of transmission dip) as a function of analyte refractive index of the nanoprism enhanced fiber taper. (a) Low particle density, (b) high particle density. In both plots, the circles refer to the very first conducted measurements, the squares to subsequent measurements after stabilization, which were then used to determine the RI sensitivity (dashed lines). The solid lines are guides-to-the-eye, and the inset in (b) shows the dependence of the localized plasmon resonance wavelength on analyte index of the nanoprisms in solution.

way by combining centrifugation and re-dilution and measuring the spectral distribution of the solution extinction (see supplementary material,⁵¹ Sec. II, optical characterization).

IV. EXPERIMENTAL RESULTS

To analyze the properties of our plasmonic taper on the basis of Eq. (3), we determined at first the extinction cross section of the silver nanoprisms ensemble in water (see supplementary material,⁵¹ Sec. II, optical characterization). We found that the nanoprism ensemble has a rather broadband distribution of σ with a peak resonance wavelength of 670 nm and a maximum cross section of $\sigma_{\max,lg} = 6.9 \times 10^{-4} \mu\text{m}^2$ (Fig. 3(a)), referring to the natural logarithm as defined in Eq. (4), $\sigma_{\max,ln} = 15.8 \times 10^{-4} \mu\text{m}^2$. Compared to typical gold nanosphere systems, the spectral broadness of the investigated ensemble here is comparably large (about 250 nm (FWHM)), which can be attributed to the size distribution of the nanoprisms, leading to a distribution of LSPR wavelength and hence to a spectral broadening of the linewidth. This size distribution is also the reason why the evolution of the extinction coefficient cannot be approximated by a single Lorentzian oscillator function.

To understand the transmission properties of our plasmonic taper, we used Eq. (4) to fit the measured transmission curve in the case of a water analyte using λ_R , P_0 , and N as fitting parameters. It is important to note that in the case of the plasmonic taper the nanoprisms are in fact immobilized on glass and thus a spectral shift of the LSPR is expected compared to the measured resonance of the NPs in solution, i.e., justifies using λ_R as fit parameter ($\sigma = \sigma_t(\lambda_R - \Delta\lambda)$). We observe that the experimentally measured transmission curve is accurately represented by Eq. (4) when using $P_0 = 0.97 \text{ mW}$, $N = 73.7 \text{ NP}/\mu\text{m}^2$, and $\lambda_R = 739.1 \text{ nm}$ (inset of Fig. 3(b), determination includes the above mentioned reduced dimensionality of the plasmonic taper), which is within the experimental error margins of the NP density. It needs to be pointed out that we only obtain a good agreement of model and experimental data if we take into account the spectral distribution of the effective mode, whereas a constant value of A_{eff} leads to an insufficient description particularly at the red side of the LSPR.

Using these fit parameters we calculated the modal extinction coefficient using Eq. (3), revealing that our meNP-enhanced taper has a peak resonance loss of the order of 0.98 dB/cm (Fig. 3(b)), lying within the expected attenuation range. Therefore our transmission model allows determining the modal attenuation of meNP-taper system, which is the key parameter of any waveguide system, under measurement conditions and without destroying the sample (as it would be the case if the cut back method is employed).

In a next step we investigated the behavior of the taper transmission for different analyte RIs in the cases of high and low nanoprism density (Fig. 4). We measure in both cases that higher analyte

RI lead to a shift of the transmission dips to longer wavelength, which results from the red-shifting LSPRs. Moreover we observe substantially deeper transmission dips for larger nanoprism densities compared to low particle coverage. For instance, in the case of $n_{\text{analyte}} = 1.383$, a depth of ≈ 2.5 dB is measured for the low coverage, whereas the high nanoprism density results in a transmission dip of ≈ 20 dB. This clearly shows that the plasmonic taper concept is capable of investigating various meNP densities using the same waveguide.

The RI sensitivity of the nanoprisms in solution was determined to 475 nm/RIU (inset of Fig. 5(b), for experimental details see supplementary material,⁵¹ Sec. II, optical characterization), which is significantly higher than that of many used NP-systems such as gold nanospheres (~ 50 nm/RIU) or gold nanocubes (~ 80 nm/RIU).

For the plasmonic taper, the evaluation of the measured data showed that the system undergoes a change after the first measurement series, i.e., after the first contact to the glucose solution, imposing a red-shift of the LSPR (Fig. 5). After the first series the plasmonic taper stabilizes and no further changes in λ_R were observed. The reason for the first initial change remains unclear to us and will be targeted in future studies. In the case of a high particle concentration (“long” immobilization time, Fig. 5(b)) we obtain a sensitivity of 892 nm/RIU, which represents the highest value reported for plasmonic optical taper so far and is substantially higher than the sensitivity of the bulk solution (475 nm/RIU, inset of Fig. 5(b)). This clearly shows that tapers provide a unique pathway for achieving highly sensitive devices on a monolithic waveguide platform. As we will discuss in a qualitative example in Sec. V (Fig. 6(b)), these high values are associated with neighboring NPs in the case of high particle density. In case the interparticle distance is larger (means a lower particle density), Fig. 5(a), we measure a lower sensitivity of 385 nm/RIU, which is comparable to that of the bulk solution.

V. QUALITATIVE SIMULATIONS

To gain a qualitative understanding of the high sensitivity values observed in the experiments, we simulate a simplified geometry consisting of a single silver nanodisk (diameter $d = 60$ nm, thickness 10 nm) on a planar slab waveguide (core silica of thickness $17 \mu\text{m}$, cladding water) using a combination of analytic mode field expressions and finite-element based scattering, in which the LSPR is excited by the guided waveguide mode (inset of Fig. 6, dielectric functions from Refs. 52 and 53). Simulating the realistic structure would require considering all particle orientations that are

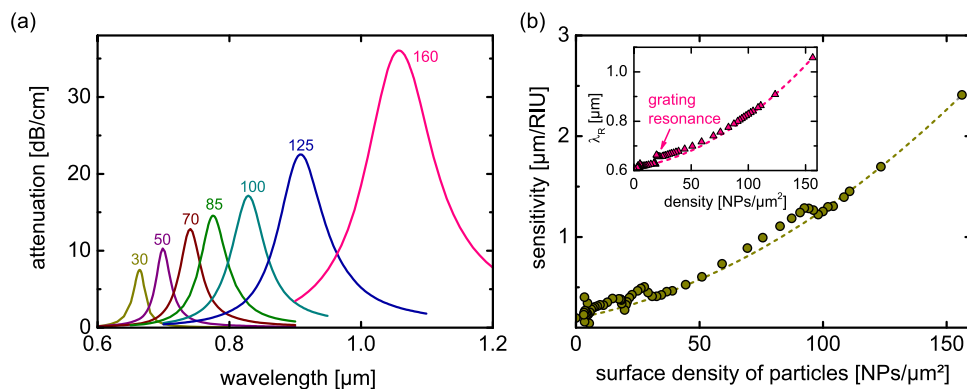


FIG. 6. Simulations of the optical properties of the plasmonic fiber taper calculated using the FEM model (TE-polarization). To reveal the qualitative behavior of the nanoparticle enhanced taper, spherical silver nanoparticles with a diameter of 60 nm are assumed. A constant analyte index of 1.33 is assumed here. (a) Spectral distribution of the modal attenuation for various nanoparticle densities (respective density values are indicated by the numbers on the top of the respective curve). (b) Corresponding refractive index sensitivity (determined at the resonance position (inset), i.e., point of highest attenuation) as a function of nanoparticle surface density. The dashed curve refers to a fitting curve with a square dependence on particle density. The non-trivial curve evolution particularly at small densities can be attributed to grating resonances.

experimentally possible and shapes, which requires a full statistical analysis and is out of the scope of this contribution.

Due to the large taper diameter (17 μm), the taper curvature at the location of the NP can be neglected and the lowest taper mode (HE_{11} -mode) then corresponds to the lowest TE or TM mode of the planar waveguide or a superposition of both depending on the azimuthal position of the particle, i.e., the relative orientation angle ϕ . Various NP densities are considered by assuming periodic boundary conditions (imposing interparticle interaction) and different gap sizes between two neighboring NPs g . The size of the simulation volume is $d + g$ in both directions, leading to $N = 1/(d + g)^2$. We have calculated the electric field distributions of the TE and TM modes analytically⁵⁴ and used them as background field distributions in the mentioned simulation volume for obtaining the scattered fields (in Comsol scattered field mode). The FEM simulations yield the scattered and total fields, and by integrating the corresponding Poynting vectors we obtain the scattered and absorbed power from which we can calculate the corresponding modal attenuation induced by one single particle γ_s . The RI sensitivity has been obtained by two identical sets of simulations assuming an analyte RI of 1.33 in one set and 1.34 in the other set. The simulations show that the LSPR excitation in TM polarization ($\vec{E}_{\text{trans}} \parallel z$) γ_s is much smaller (by a factor >2) compared to the TE case ($\vec{E}_{\text{trans}} \perp z$) and the spectral peak loss position is always <700 nm. Therefore, the TE-attenuation is the dominating contribution and is analyzed in more detail.

The attenuation spectra (Fig. 6(a)) show maxima that shift to longer wavelengths (Fig. 6(b)) with increasing amplitude when the particle density increases—a behavior that was also observed in structures such as nanoparticle chains and layers of gold nanospheres.^{1,55} As suggested by Fig. 6(b) the RI sensitivity significantly increases (more than a factor of 10) for higher particle density, which overall is a result of increasing interparticle interaction. This effect can be qualitatively understood by the following toy-model: We can approximate our particles as flat ellipsoids with a polarizability in the quasistatic limit given by Ref. 41 $\alpha_p = V(\epsilon_m - \epsilon_d)/(\epsilon_m + L(\epsilon_m - \epsilon_d))$ with the metal and surrounding dielectric permittivities ϵ_m and ϵ_d , the particle volume V , and the depolarization factor L . Plasmon resonances appear for vanishing real parts of the denominator. Assuming a Drude ansatz for ϵ_m and the condition $L \ll 1$, we obtain $\lambda_R \approx \lambda_p n_d / \sqrt{L}$ and $S \approx \lambda_p / \sqrt{L}$ (plasma wavelength of silver $\lambda_p = 137$ nm, dielectric refractive index n_d), showing that the sensitivity strongly depends on depolarization. Here, L accounts for the depolarization field that is oriented antiparallel to the polarization vector inside the particle. For a single isolated particle, the depolarization field is entirely caused by the surface charges induced by the incident wave. In case of arrays of particles, neighboring particles impose an additional contribution to the depolarization field resulting from the stray fields of the other particles. The strongest effects on the depolarization field result from the next neighbors in the direction of the polarization of the exciting field. Therefore, the effect of interaction, i.e., the increasing sensitivity for denser ensembles, can be qualitatively interpreted as a reduced depolarization factor (i.e., increasing depolarization field).

This is in correspondence with the experimental observation and explains that we observe higher sensitivity values for higher NP coverages (Fig. 6(b)). The simulated data points scatter around a quadratic polynomial curve. The latter can be related to the quasistatic model which is a good approximation for small ($\ll \lambda$) particle distances (i.e., large particle densities) as well as for single particles (zero density).

In the intermediate domain the periodic particle arrangement can act as a grating with additional resonances that cause deviations from the smooth quadratic dependence. However, these grating effects are not relevant for our experimental situation as there is no periodic arrangement, i.e., the distribution of NPs is entirely statistic.

VI. CONCLUSION AND OUTLOOK

Here we have introduced a new type of monolithic LSPR waveguide sensor based on the combination of an adiabatic optical fiber taper and immobilized gold-reinforced silver nanoprisms, showing refractive index sensitivities up to 900 nm/RIU. This result represents the highest value reported so far for a fiber optic sensor using the LSPRs of metallic nanoparticles and exceeds that of the corresponding bulk solution by a factor of two. The overall idea relies on the LSPR of the

interacting nanoparticles being excited by the evanescent field of the propagating mode, leading to a change of the transmission through the taper. This key feature of our system is that it allows accessing nanoparticle density so high that the particle interacts significantly, which substantially increases the sensitivity. This situation of interacting nanoparticles is typically difficult to achieve, whereas the taper allows precise tuning of the fraction of evanescent field outside the taper. As a result, we are able to access extremely high NP densities allowing LSPRs of neighboring NPs to interact imposing the observed high sensitivity values.

To understand the physics of our system we conducted qualitative scattering simulations revealing that the high sensitivity values are associated with interparticle interactions in case the nanoparticle density on the taper surface is high. In addition, we introduce a fitting model which explains the interaction of LSPR and taper mode on the basis of light extinction and extracting key characteristics of the plasmonic taper such as the modal attenuation. This model also shows that changing the taper geometry principally allows accessing two orders of magnitude of particle concentrations.

Since the LSPRs are detected via measuring the transmission, our system represents a highly integrated and straightforward-to-use approach, which has the potential to give rise to a full monolithic sensor for wavelength interrogation being compatible with fiber circuitry. The taper and the NP immobilization are straightforward to conduct and, due to mm-long interaction length, our sensor is of macroscopic scale, making it highly attractive within areas such as biophotonics, environmental science, or medicine. Next steps will include applying our sensor to a biologically relevant system to specifically detect chemical processes such as DNA binding events for disease diagnostics.

The application range of the extinction model introduced here (e.g., Eq. (1)) is rather general and is not restricted to cylindrical tapers. Therefore we believe that our findings will be important for all kinds of sensors relying on a coupling of a waveguide mode and LSPR, which is particularly important for systems using microstructured or even photonic crystal fibers.

ACKNOWLEDGMENTS

This work was funded by the Thuringian State Ministry for Economics, Labor, and Technology (Project No. 2012FGR0013) supported by the European Social Funds (ESF) and the Open Access fund of the Leibniz Association.

- ¹ S. A. Maier, M. L. Brongersma, P. G. Kik, and H. A. Atwater, *Phys. Rev. B* **65**(19), 193408 (2002).
- ² R. Spittel, P. Uebel, H. Bartelt, and M. A. Schmidt, *Opt. Express* **23**, 12174–12188 (2015).
- ³ P. Uebel, M. A. Schmidt, H. W. Lee, and P. S. J. Russell, *Opt. Express* **20**, 28409–28417 (2012).
- ⁴ S. A. Maier and H. A. Atwater, *J. Appl. Phys.* **98**(1), 011101 (2005).
- ⁵ W. J. Cho, A. Jung, S. Han, S. M. Lee, T. Kang, K. H. Lee, K. C. Choi, and J. K. Kim, *NPG Asia Mater.* **7**, e167 (2015).
- ⁶ G. Y. Chen, I. Roy, C. H. Yang, and P. N. Prasad, *Chem. Rev.* **116**(5), 2826–2885 (2016).
- ⁷ M. A. Schmidt, D. Y. Lei, L. Wondraczek, V. Nazabal, and S. A. Maier, *Nat. Commun.* **3**, 1108 (2012).
- ⁸ P. Kvasnicka and J. Homola, *Biointerphases* **3**(3), FD4–FD11 (2008).
- ⁹ A. Csaki, M. Thiele, J. Jatschka, A. Dathe, D. Zopf, O. Stranik, and W. Fritzsche, *Eng. Life Sci.* **15**(3), 266–275 (2015).
- ¹⁰ T. J. Wang, C. W. Tu, and F. K. Liu, *IEEE J. Sel. Top. Quantum Electron.* **11**(2), 493–499 (2005).
- ¹¹ L. He, M. D. Musick, S. R. Nicewarner, F. G. Salinas, S. J. Benkovic, M. J. Natan, and C. D. Keating, *J. Am. Chem. Soc.* **122**(38), 9071–9077 (2000).
- ¹² X. H. Huang, S. Neretina, and M. A. El-Sayed, *Adv. Mater.* **21**(48), 4880–4910 (2009).
- ¹³ A. M. Gobin, M. H. Lee, N. J. Halas, W. D. James, R. A. Drezek, and J. L. West, *Nano Lett.* **7**(7), 1929–1934 (2007).
- ¹⁴ C. R. Patra, R. Bhattacharya, D. Mukhopadhyay, and P. Mukherjee, *J. Biomed. Nanotechnol.* **4**(2), 508–514 (2008).
- ¹⁵ K. M. Mayer and J. H. Hafner, *Chem. Rev.* **111**(6), 3828–3857 (2011).
- ¹⁶ H. J. Chen, X. S. Kou, Z. Yang, W. H. Ni, and J. F. Wang, *Langmuir* **24**(10), 5233–5237 (2008).
- ¹⁷ D. Y. Lei, A. I. Fernandez-Dominguez, Y. Sonnefraud, K. Appavoo, R. F. Haglund, J. B. Pendry, and S. A. Maier, *ACS Nano* **6**(2), 1380–1386 (2012).
- ¹⁸ T. Schneider, N. Jahr, J. Jatschka, A. Csaki, O. Stranik, and W. Fritzsche, *J. Nanopart. Res.* **15**(4), 1531 (2013).
- ¹⁹ S. Linden, A. Christ, J. Kuhl, and H. Giessen, *Appl. Phys. B: Lasers Opt.* **73**(4), 311–316 (2001).
- ²⁰ S. Linden, J. Kuhl, and H. Giessen, *Phys. Rev. Lett.* **86**(20), 4688–4691 (2001).
- ²¹ T. Wieduwilt, K. Kirsch, J. Dellith, R. Willsch, and H. Bartelt, *Plasmonics* **8**(2), 545–554 (2013).
- ²² J. Villatoro, D. Monzon-Hernandez, and E. Mejia, *Appl. Opt.* **42**(13), 2278–2283 (2003).
- ²³ D. Monzon-Hernandez and J. Villatoro, *Sens. Actuators, B* **115**(1), 227–231 (2006).
- ²⁴ N. Diaz-Herrera, A. Gonzalez-Cano, D. Viegas, J. L. Santos, and M. C. Navarrete, *Sens. Actuators, B* **146**(1), 195–198 (2010).
- ²⁵ T. Wieduwilt, A. Tuniz, S. Linzen, S. Goerke, J. Dellith, U. Hubner, and M. A. Schmidt, *Sci. Rep.* **5**, 17060 (2015).

- ²⁶ H. Y. Lin, C. H. Huang, G. L. Cheng, N. K. Chen, and H. C. Chui, *Opt. Express* **20**(19), 21693–21701 (2012).
- ²⁷ S. K. Srivastava, V. Arora, S. Sapra, and B. D. Gupta, *Plasmonics* **7**(2), 261–268 (2012).
- ²⁸ W. T. Hsu, W. H. Hsieh, S. F. Cheng, C. P. Jen, C. C. Wu, C. H. Li, C. Y. Lee, W. Y. Li, L. K. Chau, C. Y. Chiang, and S. R. Lyu, *Anal. Chim. Acta* **697**(1-2), 75–82 (2011).
- ²⁹ S. F. Cheng and L. K. Chau, *Anal. Chem.* **75**(1), 16–21 (2003).
- ³⁰ L. K. Chau, Y. F. Lin, S. F. Cheng, and T. J. Lin, *Sens. Actuators, B* **113**(1), 100–105 (2006).
- ³¹ J. S. Crosby, D. Lucas, and C. P. Koshland, *Sens. Actuators, B* **81**, 938–942 (2013).
- ³² Y. L. Shao, S. P. Xu, X. L. Zheng, Y. Wang, and W. Q. Xu, *Sensors* **10**(4), 3585–3596 (2010).
- ³³ J. Luo, J. Yao, Y. G. Lu, W. Y. Ma, and X. Y. Zhuang, *Sensors* **13**(3), 3986–3997 (2013).
- ³⁴ L. Rindorf and O. Bang, *Opt. Lett.* **33**(6), 563–565 (2008).
- ³⁵ D. K. C. Wu, B. T. Kuhlmeier, and B. J. Eggleton, *Opt. Lett.* **34**(3), 322–324 (2009).
- ³⁶ H. W. Lee, M. A. Schmidt, P. Uebel, H. Tyagi, N. Y. Joly, M. Scharrer, and P. S. Russell, *Opt. Express* **19**(9), 8200–8207 (2011).
- ³⁷ L. V. Nguyen, K. Hill, S. Warren-Smith, and T. Monro, *Sens. Actuators, B* **221**, 320–327 (2015).
- ³⁸ Z. L. Ran, Y. J. Rao, J. Zhang, Z. W. Liu, and B. Xu, *J. Lightwave Technol.* **27**(23), 5426–5429 (2009).
- ³⁹ T. Wieduwilt, J. Dellith, F. Talkenberg, H. Bartelt, and M. A. Schmidt, *Opt. Express* **22**(21), 25333–25346 (2014).
- ⁴⁰ S. C. Warren-Smith, R. Kostecki, L. V. Nguyen, and T. M. Monro, *Opt. Express* **22**(24), 29493–29504 (2014).
- ⁴¹ C. F. Bohren and D. R. Huffman, *Absorption and Scattering of Light by Small Particles* (Wiley-VCH Verlag GmbH, Weinheim, 1998).
- ⁴² F. Warken, E. Vetsch, D. Meschede, M. Sokolowski, and A. Rauschenbeutel, *Opt. Express* **15**(19), 11952–11958 (2007).
- ⁴³ X. C. Yu, B. B. Li, P. Wang, L. M. Tong, X. F. Jiang, Y. Li, Q. H. Gong, and Y. F. Xiao, *Adv. Mater.* **26**(44), 7462–7467 (2014).
- ⁴⁴ J. A. Snyder and J. D. Love, *Optical Waveguide Theory* (Chapman and Hall, London, New York, 1983).
- ⁴⁵ F. Le Kien, J. Q. Liang, K. Hakuta, and V. I. Balykin, *Opt. Commun.* **242**(4-6), 445–455 (2004).
- ⁴⁶ P. Mulvaney, T. Linnert, and A. Henglein, *J. Phys. Chem.* **95**(20), 7843–7846 (1991).
- ⁴⁷ T. Pal, T. K. Sau, and N. R. Jana, *Langmuir* **13**(6), 1481–1485 (1997).
- ⁴⁸ D. Aherne, D. E. Charles, M. E. Brennan-Fourmet, J. M. Kelly, and Y. K. Gun'ko, *Langmuir* **25**(17), 10165–10173 (2009).
- ⁴⁹ M. M. Shahjamali, M. Salvador, M. Bosman, D. S. Ginger, and C. Xue, *J. Phys. Chem. C* **118**(23), 12459–12468 (2014).
- ⁵⁰ K. E. Lee, A. V. Hesketh, and T. L. Kelly, *Phys. Chem. Chem. Phys.* **16**(24), 12407–12414 (2014).
- ⁵¹ See supplementary material at <http://dx.doi.org/10.1063/1.4953671> for preparation and characterization of the silver nanoprisms as well as the preparation of the nanoparticles-covered optical fiber probe.
- ⁵² P. B. Johnson and R. W. Christy, *Phys. Rev. B* **6**(12), 4370–4379 (1972).
- ⁵³ E. D. Palik, *Handbook of Optical Constants of Solids* (Academic Press, London, 1998).
- ⁵⁴ T. Tamir, G. Griffel, and H. L. Bertoni, *Guided-Wave Optoelectronics: Device Characterization, Analysis, and Design* (Springer, 1995).
- ⁵⁵ E. Martinsson, B. Sepulveda, P. Chen, A. Elfving, B. Liedberg, and D. Aili, *Plasmonics* **9**(4), 773–780 (2014).